Measurement report: Comparison of wintertime individual particles at ground level and above the mixed layer in urban Beijing

Wenhua Wang[1,2,3], Longyi Shao[1*], Claudio Mazzoleni[3], Yaowei Li[1], Simone Kotthaus[4], Sue Grimmond[4], Janarjan Bhandari[3], Jiaoping Xing[1,5], Xiaolei Feng[1], Mengyuan Zhang[1], Zongbo Shi[6]

1. State Key Laboratory of Coal Resources and Safe Mining & College of Geosciences and Surveying Engineering, China University of Mining and Technology, Beijing, 100083, China

2. School of Resources and Materials, Northeastern University at Qinhuangdao, Qinhuangdao, 066004, China

3. Atmospheric Sciences Program & Physics Department, Michigan Technological University, Houghton, 49931, USA

4. Department of Meteorology, University of Reading, Reading, RG6 6BB, UK

5. School of Forestry, Jiangxi Agricultural University, Nanchang, 330045, China

6. School of Geography Earth and Environmental Sciences, the University of Birmingham, Birmingham, B15 2TT, UK

* Corresponding author: ShaoL@cumtb.edu.cn

Abstract:

Beijing has been suffering from frequent severe air pollution events, with concentrations affected significantly by the mixed layer height. Major efforts have been made to study the physico-chemical properties, compositions, and sources of aerosol particles at ground level. However, little is known about the morphology, elemental composition, and mixing state of aerosol particles above the mixed layer. In this work, we collected individual aerosol particles simultaneously at ground level (2 m above ground) and above the mixed layer in urban Beijing (within the Atmospheric Pollution and Human Health in a Chinese Megacity (APHH-Beijing) 2016 winter campaign). The particles were analyzed off-line by transmission electron microscopy coupled with energy dispersive X-ray spectroscopy. Our results showed that the relative number contribution of mineral particles to all measured particles was much higher during non-haze periods (42.5%) than haze periods (18.1%); on the contrary, internally mixed particles contributed more during haze periods (21.9%) than non-haze periods (7.2%) at ground level. In addition, more mineral particles were found at ground level than above the mixed layer height. Around 20% of individual particles showed core-shell structures during haze periods, whereas only a few core-shell particles were observed during non-haze periods (2%). The results showed that the particles above the mixed layer were more aged with a larger proportion of organic particles originated from coal combustion. Our results indicate that a large fraction of the airborne particles above the mixed layer come from surrounding areas influenced by coal combustion activities. This source contributes to the surface particle concentrations in Beijing when polluted air is mixed down to the ground level.

Keywords: haze; individual particle; organic particle; core-shell structure; mixed layer.

1. Introduction

Atmospheric aerosols emitted from anthropogenic or natural sources are composed of a variety of chemical components (e.g., organic matter, black carbon, nitrate, sulfate, ammonium, metals, mineral dust) (Merikallio et al., 2011; Guo et al., 2014; Wang et al., 2016; Peng et al., 2016; Shao et al., 2017; Tao et al., 2017). Anthropogenic aerosols have received increasing attention in recent decades due to their effects on climate and the environment. In fact, anthropogenic aerosols affect climate through cloud condensation nuclei activity (Kerminen et al., 2012), hygroscopic growth (Brock et al., 2016), and light scattering and absorption (Jacobson, 2001; Bond and Bergstrom, 2006; Merikallio et al., 2011; China et al., 2013; Peng et al., 2016; Bhandari et al., 2019b). They can also have adverse effects on human health, for example, by carrying toxic and carcinogenic compounds (Chen et al., 2013; Shao et al., 2016, 2017). High concentrations of aerosol particles in urban air can cause cardiovascular, respiratory, and even nervous system diseases (Xia et al., 2018; De Marco et al., 2019; Shou et al., 2019). It is suggested that outdoor air pollution causes 3.3 million people premature deaths worldwide each year (Lelieveld et al., 2015). Atmospheric aerosol particles also affect regional and global geochemical cycles as they are transported over long distances (Heald et al., 2006; Weijun Li et al., 2017; Rodriguez-Navarro et al., 2018).

Recently, China has suffered from severe air pollution conditions, like other countries undergoing rapid social and economic development (Huang et al., 2014). In China, urban air pollution is characterized by frequent occurrence of haze events, high $PM_{2.5}$ mass level, and expanded haze areas (Guo et al., 2014; Huang et al., 2014; Sun et al., 2014). For example, the maximum hourly average $PM_{2.5}$ mass concentrations in winter in Beijing reached more than 1000 $\mu g\ m^{-3}$ (Li et al., 2017a; Zhang et al., 2017), 40 times above the safe level of 25 $\mu g\ m^{-3}$ recommended by the World Health Organization (WHO).

As the megacity capital, Beijing has received much attention being one of the most polluted cities in China. Atmospheric researchers have been studying aerosol particles to understand haze formation in China (Sun et al., 2013; Huang et al., 2014; Zhou et al., 2018b). Measurements and model analyses highlight the key roles of secondary aerosol formation by trace gases (e.g., volatile organic compounds, and SO_2, NO_x) and stagnant meteorological conditions in the regional haze formation (Wang et al., 2013; Guo et al., 2014; Huang et al., 2014).

63   Because the characterization of aerosol particles is mainly focused on surface level

64   observations, the understanding of aerosol properties at higher altitudes in urban areas is still

65   insufficient (Zhou et al., 2018a). Vertical differences between precursors, oxidants and temperature

66   gradients might influence gas-particle partitioning and heterogeneous reactions of N_2O_5 (Zhou et

67   al., 2018a). Previous measurements at the Institute of Atmospheric Physics (IAP) meteorological

68   tower in Beijing showed complex vertical distributions of particulate matter and gaseous pollutants

69   (Meng et al., 2008; Sun et al., 2015; Wang et al., 2018; Zhou et al., 2018b). However, most of these

70   studies focused on non-refractory submicron species. Research showed that the mixed layer height

71   (MLH) could explain some of the vertical difference of aerosol particle chemical composition (Sun

72   et al., 2015; Wang et al., 2018; Zhang et al., 2012). For example, vertical distributions of aerosol

73   particles were more uniform during periods with higher MLH (Wang et al., 2018). As heavily

74   increased air pollution could reduce boundary layer heights by diminishing incoming solar energy

75   and therefore by weakening vertical turbulence, near-surface aerosol concentrations become

76   elevated (Petaja et al., 2016). Moreover, the upper layer particles could influence those below the

77   MLH by downward entrainment or mixing plumes, making the lower layer particles more complex

78   (Wehner et al., 2010; Platis et al., 2015; Qi et al., 2019). Previous studies showed that the particles

79   above the MLH considerably influenced cloud formation (Carnerero et al., 2018) and showed strong

80   aerosol-radiation effect (Bond and Bergstrom, 2006). The differences in aerosol types at ground

81   level and at higher altitudes could lead to large differences in aerosol direct forcing estimates

82   (Ramanathan et al., 2002; Li et al., 2010). The vertical difference of aerosol particles also increases

83   the uncertainties in the assessment of the climate system (Li et al., 2017b). Therefore, a detailed

84   knowledge of the vertical distribution and chemical composition of aerosols is important for

85   understanding the impact on climate and the aerosol evolution process (Zhang et al., 2009; Wang et

86   al., 2018).

87   Vertical comparisons of individual aerosol particles and their morphologies, mixing states, and

88   elemental compositions are very limited. Transmission Electron Microscopy (TEM) can provide

89   detailed individual particle characterization and help to explain heterogeneous reactions and aging

90   process (Li et al., 2016a). In this study, we compare particles simultaneously collected at ground

91   level and above the MLH based on the meteorological tower at IAP in Beijing, as part of the UK-

92   CHINA atmospheric pollution and Human Health (APHH) 2016 winter campaign.

93   **2.   Experimental**

94   **2.1.   Aerosol sampling**

95   Individual aerosol samples were collected at the tower division of IAP, Chinese Academy of

96   Science (39°58′N, 116°22′E), in Beijing from 1 to 9 December of 2016. The site, located between

97   the north 3rd and 4th ring roads in Beijing, is influenced by surrounding and regional traffic, and

98   commercial, as well as, residential activities (Sun et al., 2016). There is a highway 250 m East of

99   IAP.

100   Two DKL-2 single stage cascade impactors, with a 0.5-mm-diameter jet nozzle and a flow rate

101   of 1 L min^{-1} were used. The sampler collection efficiency is ~ 100% at an aerodynamic diameter of

102   0.5 μm if the particle density is 2 g·cm^{-3} (Li et al., 2016b). Copper (Cu) TEM grids, coated with

103   carbon film (300-mesh; Tianld Co.; Beijing, China), were used to collect the aerosol samples. The

104   sampling duration varied from 30 seconds to less than 5 minutes depending on the air pollution load.

105   Simultaneous observations at ground level (Z1; 2 m above ground) and an elevated altitude (Z2;

106   280 m above ground) enabled us to obtain the vertical profile of the particles. The collected samples

107   were stored in a dry plastic tube and placed in an air dryer to minimize particle changes before

108   analysis.

109   Automatic Lidar and Ceilometer (ACL) observations of attenuated backscatter were conducted

110   at the site using a Vaisala CL31 sensor. Measurements were corrected to account for instrument-

111   related background and near range artefacts (Kotthaus et al., 2016). The MLH was derived from

112   profile measurements using the automatic CABAM algorithm (Kotthaus and Grimmond, 2018).

113   Since the TEM samples were collected for less than 5 minutes, the MLH at 15 min resolution was

114   used to determine whether the Z2 observations were located within the MLH or above the MLH

115   (Shi et al., 2019).

116   Samples were obtained during the periods shown (solid dots and dashed lines) in Fig. 1.

117   Detailed sample information is provided in Table 1. Other measurements including PM$_{2.5}$, SO$_2$, NO$_2$,

118   and O$_3$ mass concentrations at ground level were obtained from the Olympic Park monitor site,

119   which is the closest national air quality monitor station to IAP (~1.5 km) (Shi et al., 2019). City

120   average temperature (T) and relative humidity (RH) at ground level were obtained from the Ministry

121 of Ecology and Environment of China (https://www.aqistudy.cn/). In this study, the particles were

122 all collected in the morning and midnight when the MLH was the lowest and the height of the tower

123 could reach the MLH at that time.

2.2. Individual particle analysis

125 Individual particles were analyzed using a JEOL JEM-2800 TEM at an accelerating voltage of

126 200 kV. The morphology and mixing state of individual particles were determined from the TEM

127 images. Semi-quantitative elemental composition was determined using Energy Dispersive X-ray

128 Spectroscopy (EDS), by which elements heavier than Boron (Z>5) can be detected. Cu was not

129 included because the TEM grids were made of copper. The EDS collection duration of each

130 individual particle was about 15 s to reduce damage of particles from the electron beam. For most

131 particles, only one spectrum of each particle was collected and the spot size of beam would be

132 adjusted according to the size of the particles. Therefore, we obtained the average elemental

133 compositions of each particle. However, more than one spots per particle were collected if the

134 particles were inhomogeneous particles according to the TEM images. The aerosol particles were

135 not evenly distributed on the TEM grids; the coarser particles occurred near the center and the finer

136 particles occurred on the periphery. To ensure a representative data analysis, three or four meshes

137 from the center to the periphery were selected and analyzed. The projected areas of individual

138 particles were determined using the Image-J software (Schneider et al., 2012), which was commonly

139 used for counting and measuring the projected area of atmospheric particles acquired by electron

140 microscopes (Unga et al., 2018). First, the gray-scale images of the particles were converted into

141 binary images, in which black pixels represented the particles and white pixels represented the

142 background. The area equivalent diameters (D_{Aeq}) of the particles are calculated by the following

143 formula: $D_{Aeq}= 2 \cdot (A/\pi)^{1/2}$, where A is the projected area of the particles shown in the TEM images

144 (Bhandari et al., 2019a). Most of the particles with diameter larger than 100 nm were analyzed in

145 this study.

3. Results and discussions

3.1. Mass concentration of air pollutants

148 The temporal variations of different air pollutants and meteorological conditions at ground

149 level are shown in Fig. 1. The hourly averaged $PM_{2.5}$ mass concentration at the Olympic Park

150 monitoring site ranged from 3 to 530 µg m^{-3}, with a sample period average of 113.3 µg m^{-3},

151 significantly exceeding the safe level of 75 µg m^{-3} according to the Chinese National Ambient Air

152 Quality Standard (GB3095-2012). The MLH ranged from 54 to 1496 m, with an average of 397 m.

153 The MLH showed obvious diurnal variation. The hourly mean RH ranged from 17% to 97%, with

154 a 9 day mean of 50.3%. The RH and PM$_{2.5}$ were positively correlated (correlation coefficient=0.75;

155 Fig. S1) according to the 216 groups of hourly data, suggesting that higher RH favors the formation

156 of haze (Sun et al., 2014;Wang et al., 2016). As expected, RH and temperature were negatively

157 correlated (correlation coefficient=-0.51; Fig. S2). The variation trend of SO$_2$ was similar to that of

158 NO$_2$. However, the average concentration of NO$_2$ (83.2 µg m^{-3}) was nearly 5.5 times higher than

159 that of SO$_2$ (15.2 µg m^{-3}). The concentration of O$_3$ showed a different trend compared with NO$_2$ and

160 SO$_2$ (Fig. 1), with a 9 days hourly mean concentration of 20 µg m^{-3}.

161 **3.2. Classification and mixing state of individual particles**

162   Aerosol particles are classified using their morphologies and elemental compositions into

163 seven main types, namely: 1) primary organic aerosols (POA), 2) sulfur-rich (S-rich) particles, 3)

164 soot particles, 4) mineral particles, 5) metal particles, 6) internally mixed organic and sulfur-rich

165 particles (OP-S), and 7) other mixed particles. The detailed characteristics of each particle type are

166 shown in Table 2.

167   POA particles are mainly composed of C and O, usually with a small amount of Si, S, Cl, and

168 K. POA particles are relatively stable under the electron beam irradiation. Based on the

169 morphologies, POA particles can be further divided into spherical (Fig. 2a) and irregularly shapes

170 (Fig. 2b). They are mainly from combustion process of biomass and fossil fuel (Li et al., 2016a; Liu

171 et al., 2021).

172   S-rich particles (Figs. 2c and 2d) are mainly composed of O, S, and N, and sometimes also

173 contain some amount of K. S-rich particles are beam-sensitive and volatilize under strong beam

174 irradiation. S-rich particles generally represent secondary inorganic components (e.g., SO$_4^{2+}$, NO$_3^-$

175 and NH$_4^+$) (Xu et al., 2019).

176   Soot particles are mainly composed of C, minor amount of O, and sometimes Si. Soot particles

177 consist of a number of C-dominated spherical monomers less than 100 nm in diameter (Figs. 2e and

178 2f) and can be easily identified under high-resolution TEM (Buseck et al., 2014; Bhandari et al.,

2017). Soot particles, stable under the electron beam, show chain-like or compact morphologies in the atmosphere (Sorensen et al., 2001; Adachi et al., 2007; China et al., 2013, 2015; Bhandari et al., 2019a). Soot particles are mainly from incomplete combustion of biomass and fossil fuel.

Metal particles (Figs. 2g and 2h) and mineral particles (Fig. 2i) are stable under the beam irradiation. Mineral particles are mostly irregularly shaped containing crustal elements (e.g., Si, Al, Ca, Fe, Na, K, Mg, Ti, and S) in addition to O. They can be generated from windblown soil dust or road dust. Metal particles are spherical or near spherical and are mainly composed of Fe, Zn, Mn, Ti, and Pb. Metal particles ae mainly originated from industries, coal-fired power plants, and oil refineries (Xu et al., 2019) or vehicle brakes (Hou et al., 2018).

Internally mixed particles (Figs. 2j-p) are particles with at least two of the above components. They usually show relative larger diameter. We further classify them as internally mixed organic and sulfur-rich particles (OP-S) (Figs. 2j-l), and other mixed particles (Figs. 2m-p).

3.3. Comparison of haze and non-haze individual particle at ground level

Haze periods are defined as hourly average $PM_{2.5}$ mass concentration greater than 75 μg m^{-3} during collection time; the rest are defined as non-haze periods. A total of 1538 individual particles among 8 samples at ground level were analyzed based on the TEM results. The relative number percentage (N(type i)/ N(total)*100) of particles in each sample was calculated. The results are provided in Table 3 and shown in Fig.3. During non-haze periods, the particles were composed of mineral particles (42.5%), POA particles (21.1%), S-rich particles (20.0%), soot particles (6.4%), other mixed particles (5.6%), metal particles (2.83%), and OP-S (1.6%) in descending order. During haze periods, the particles were composed of POA particles (28.3%), S-rich particles (23.5%), mineral particles (18.1%), OP-S (13.1%), other mixed particles (8.8%), soot particles (6.6%), and metal particles (1.7%) in descending order.

The mineral particles are mainly from re-suspended road dust, soil dust, and construction dust during non-desert transport dust episodes (Sun et al., 2006; Gao et al., 2016; Wang et al., 2017). The relative number percentage of mineral particles was much higher during non-haze periods (42.5%) than during haze periods (18.1%), as shown in Fig.3.

However, the content of mixed particles including OP-S and other mixed particles during haze periods (21.9%) was much higher than during non-haze periods (7.2%), suggesting that there was

208   more secondary aerosol formation during haze periods. High secondary aerosol formation in winter

209   in Beijing during the pollution periods was also found in previous studies (Huang et al., 2014; Sun

210   et al., 2016; Li et al., 2017a). Secondary aerosol formation was expected since the RH during the

211   haze periods were relatively higher than during non-haze periods, as shown in Table 1 and Fig.1,

212   which facilitated chemical reactions of gaseous pollutants (Liu et al., 2016; Wang et al., 2016). Also,

213   the average content of POA particles and S-rich were higher during haze periods than during non-

214   haze periods.

215   **3.4.   Comparison of individual particles at ground level and above the MLH**

216   A total of 1519 individual particles among 8 samples above the MLH were analyzed. The results

217   are provided in Table 3 and shown in Fig. 3. We found that the relative number percentage of mineral

218   particles at ground level was larger than that above the MLH. For example, mineral particles at

219   ground level and above the MLH during non-haze periods accounted for 42.5% and 23.2%,

220   respectively, and during haze periods the values are 18.1% and 9.5%, respectively. S-rich particles

221   during non-haze periods accounted for 20.0% at ground level, less than the value of 30.7% above

222   the MLH. However, not all the samples above the MLH during haze periods showed higher relative

223   number percentage of S-rich particles than at ground level. This might because some of the S-rich

224   particles above the MLH were mixed with other particles, forming mixed particles. Another reason

225   might be that higher relative number percentage of mixed particles diluted the relative number

226   percentage of S-rich particles. The mixed particles during haze periods accounted for 32.0% above

227   the MLH, higher than that of 21.9% at ground level. We also found that POA particles above the

228   MLH accounted for higher relative number percentage than at ground level, although there was

229   some variance. For example, samples 4 and 6 showed higher relative number percentage of POA

230   particles at ground level. That might because that some of the POA particles were mixed with S-

231   rich particles and OP-S showed higher relative number percentage above the MLH than at ground

232   level in samples 4 and 6. Metals and soot only accounted for a few relative number percentages in

233   all samples and they didn't show much difference at ground level and above the MLH. Particles

234   above the MLH were either transported from the surrounding areas or from ground sources. In both

235   cases, they were subject to atmospheric process, leading to their aging.

236   **3.5.   Aging of particles**

In the atmosphere, particles are subjected to aging process. During the aging process of aerosol

particles, secondary species can coat pre-existing particles (Li and Shao, 2009; Laskin et al., 2016;

Li et al., 2016b; Niu et al., 2016; Tang et al., 2016; Chen et al., 2017; Hou et al., 2018; Unga et al.,

2018; Xu et al., 2019). Using high-resolution TEM images, it is possible to identify the core-shell

structure of particles (Li et al., 2016a). For example, Figs. 4a and 4b showed S-rich particles coated

by secondary species. Figs. 4c and 4d were POA particles coated with secondary species. Figs. 4e-

h showed core-shell structured particles with some mixed particle cores. In this study, we found that

the core-shell structured particles accounted for 20% during haze periods with 17% at ground level

and 23% above the MLH, but only 2% during non-haze periods. These results demonstrated a

general trend that the core-shell structured particles during haze periods were much higher than

during non-haze periods. Also, the average D_{Aeq} of particles was larger during haze periods than

during non-haze periods as shown in Fig. S3. These results confirmed that particles during haze

periods underwent more extensive aging than during non-haze periods.

The coating of atmospheric particles is often caused by aging mechanisms such as coagulation,

condensation, and heterogeneous chemical reactions (Kahnert, 2015; Müller et al., 2017, Zhang et

at., 2012). Fig. 5 shows low magnification images of particles at ground level and above the MLH.

More core-shell particles were found above the MLH. The core/shell ratio (R), which is the ratio of

the D_{Aeq} of core to the D_{Aeq} of whole particle including the coating, has been used to evaluate the

aging process of aerosol particles in different studies (Niu et al., 2012, 2016; Hou et al., 2018). The

value of R ranged from 0 to less than 1. A smaller R value means the particles are more coated, thus

are subjected to a more extensive degree of aging (Hou et al., 2018). Because high number

percentage of core-shell structured particles were only found during haze periods, we only measured

R of core-shell structured particles during the haze periods (including the samples 2, 4, 5, 6 and 7).

Fig. 6a shows the R value of each samples during the haze periods. We can see from Fig. 6a that all

the samples showed a smaller average R value above the MLH compared with those from the ground

level. The average R value above the MLH (0.54) was smaller than ground level (0.59). Additionally,

the relative number percentage of core-shell structured particles was higher above the MLH than at

ground level, except for sample 4. These findings indicated that the particles above the MLH were

more aged than those at ground level.

266   Fig. S3 shows the total particle number-size distribution; the relative number percentage of the

267   larger size particles clearly increased when considering the coatings compared to only considering

268   the core size during haze periods. The change in optical properties due to coating was calculated in

269   various studies by using different methods (Cappa et al., 2012; Scarnato et al., 2013; Liu et al., 2015;

270   Saliba et al., 2016; Unga et al., 2018). When host particles were coated, their optical properties

271   might be amplified (Khalizov et al., 2009; Peng et al., 2016). Also, organic coating can influence

272   the hygroscopic properties and the viscosity of mixed particles (Sharma et al., 2018; Unga et al.,

273   2018), and thus can influence cloud formation activity (Kerminen et al., 2012).

274   **3.6.   Possible sources of organic particles**

275   Our results showed higher relative number percentage of POA particles both during non-haze

276   (21.1%) and haze periods (28.3%) in winter Beijing, compared with a tunnel environment (~5%),

277   where the vehicle emissions were the main pollution sources (Hou et al., 2018). Also, recent studies

278   did not find abundant POA particles in North China during Spring and Summer (Yuan et al., 2015;

279   Li et al., 2016b; Xu et al., 2019;). Instead, a larger number percentage of POA particles have been

280   found in winter using electron microscopy in previous studies, including an outflow of a haze plume

281   in East Asia (Zhu et al., 2013), a coal-burning region in China's Loess Plateau (Li et al., 2012), three

282   sampling sites in North China Plain (Chen et al., 2017) and urban and rural sites in Northeast China

283   (Xu et al., 2017; Zhang et al., 2017). These results suggested that POA particles accounted for a

284   large number percentage of the particles in north China in winter.

285   Most of the POA particles in our study were spherical or nearly spherical in shape according

286   to the projected images and they were stable under strong electron beam irradiation and appear dark

287   features in TEM images, which reflected their high thickness and refractory properties (Ebert et al.,

288   2016), suggesting that they were formed through cooling process after the biomass or fossil fuel

289   combustion pyrolysis products of volatile organic compounds were emitted into the atmosphere

290   (Wang et al., 2015; Chen et al., 2017; Zhang et al., 2017).

291   These spherical or near spherical POA particles are considered to be brown carbon (Zhang et

292   al., 2020). Brown carbon plays a significant role in atmospheric shortwave absorption and can cause

293   warming of the atmosphere (Adachi and Buseck, 2011;Hoffer et al., 2016). Some researchers have

294   found that the primary POA particles from coal combustion have more Si than those from biomass

295 burning (Li et al., 2012; Chen et al., 2017). The weight ratio of C-O-Si at ground level and above

296 the MLH is shown in Fig. 7. More coal burning related POA particles were found above the MLH.

297 Since the relative number percentage of POA particles affected by coal burning are higher above

298 the MLH than at ground level, POA particles above the MLH are not all from ground level and

299 might be originated from surrounding areas influenced by coal combustion. The results were

300 supported by the 24-h backward trajectories, which showed that air masses above the MLH during

301 haze periods were from the North and West direction of Beijing as shown in Fig. S4. It is reasonable

302 that Beijing has implemented strict air pollution controls measures, including using natural gas to

303 replace domestic coal burning. The particles above the MLH can contribute to Beijing air pollution

304 by mixing down to the ground.

305 4. Conclusions

306 Detailed morphologies and elemental compositions of individual aerosol particles at ground level

307 and above the mixed layer height were analyzed in this study. Following conclusions were achieved:

308 1) Particles were classified into primary organic particles, S-rich particles, mineral particles,

309 metal particles, soot, internally mixed organic and sulfur-rich particles, and other mixed particles.

310 Compared with non-haze periods, haze periods were associated with a relative lower number

311 percentage of mineral particles and a relative higher number percentage of mixed particles.

312 2) Compared with the aerosol samples at ground level, the samples above MLH had a lower

313 relative number percentage of mineral particles, a higher number percentage of coated particles, a

314 smaller core/shell ratio of coated particles. More coated particles and higher core/shell ratio in the

315 aerosol samples above the mixed layer suggested that the particles above the mixed layer were more

316 aged.

317 3) Relative number percentage of primary organic particles accounted for 21.1% during non-haze

318 periods and 28.3% during haze periods in winter Beijing. More primary organic particles above the

319 mixed layer were associated with coal combustion according to the C-O-Si ratio, and the long-range

320 transportation of air masses from surrounding areas has an important influence for Beijing air.

321 **Data availability:** Data used in this study are available from the corresponding author upon request
322 (ShaoL@cumtb.edu.cn)

323 **Author Contributions:** WW, LS, CM, JX and ZS conceived the manuscript. WW, YL, XF and MZ
324 conducted the sample collection and analysis. SK and SG conducted the MLH measurement. CM
325 and BJ conducted manuscript modification.

326 **Competing interest:** The authors declare no conflict of interest.

327 **Acknowledgements:** We thank Zifa Wang and Pingqing Fu at IAP for the supporting of sample
328 collection. This work was supported by National Natural Science Foundation of China (No.
329 42075107), International Cooperation Projects of National Natural Science Foundation of China
330 (No. 41571130031), China Scholarship Council (No. 201806430015), Yue Qi Scholar Fund of
331 China University of Mining and Technology (Beijing). CM and JB were supported by the U.S
332 Department of Energy (DOE), Office of Biological and Environmental Research (OBER),
333 Atmospheric System Research (#DE-SC0011935 and Grant # DE-SC0018931). ZS was supported
334 by Natural Environmental Research Council (NE/N007190/1).

Reference:

Adachi, K., Chung, S. H., Friedrich, H., and Buseck, P. R.: Fractal parameters of individual soot particles determined using electron tomography: Implications for optical properties, Journal of Geophysical Research, 112, 10.1029/2006jd008296, 2007.

Adachi, K., and Buseck, P. R.: Atmospheric tar balls from biomass burning in Mexico, J. Geophys. Res.-Atmos., 116, 7, 10.1029/2010jd015102, 2011.

Bhandari, J., China, S., Onasch, T., Wolff, L., Lambe, A., Davidovits, P., Cross, E., Ahern, A., Olfert, J., Dubey, M., and Mazzoleni, C.: Effect of Thermodenuding on the Structure of Nascent Flame Soot Aggregates, Atmosphere, 8, 10.3390/atmos8090166, 2017.

Bhandari, J., China, S., Chandrakar, K. K., Kinney, G., Cantrell, W., Shaw, R. A., Mazzoleni, L. R., Girotto, G., Sharma, N., Gorkowski, K., Gilardoni, S., Decesari, S., Facchini, M. C., Zanca, N., Pavese, G., Esposito, F., Dubey, M. K., Aiken, A. C., Chakrabarty, R. K., Moosmuller, H., Onasch, T. B., Zaveri, R. A., Scarnato, B. V., Fialho, P., and Mazzoleni, C.: Extensive Soot Compaction by Cloud Processing from Laboratory and Field Observations, Sci Rep, 9, 11824, 10.1038/s41598-019-48143-y, 2019a.

Bhandari, J., China, S., Girotto, G., Scarnato, B. V., Gorkowski, K., Aiken, A. C., Dubey, M. K., and Mazzoleni, C.: Optical properties and radiative forcing of fractal-like tar ball aggregates from biomass burning, Journal of Quantitative Spectroscopy and Radiative Transfer, 230, 65-74, 10.1016/j.jqsrt.2019.01.032, 2019b.

Bond, T. C., and Bergstrom, R. W.: Light Absorption by Carbonaceous Particles: An Investigative Review, Aerosol Science and Technology, 40, 27-67, 10.1080/02786820500421521, 2006.

Brock, C. A., Wagner, N. L., Anderson, B. E., Attwood, A. R., Beyersdorf, A., Campuzano-Jost, P., Carlton, A. G., Day, D. A., Diskin, G. S., Gordon, T. D., Jimenez, J. L., Lack, D. A., Liao, J., Markovic, M. Z., Middlebrook, A. M., Ng, N. L., Perring, A. E., Richardson, M. S., Schwarz, J. P., Washenfelder, R. A., Welti, A., Xu, L., Ziemba, L. D., and Murphy, D. M.: Aerosol optical properties in the southeastern United States in summer – Part 1: Hygroscopic growth, Atmospheric Chemistry and Physics, 16, 4987-5007, 10.5194/acp-16-4987-2016, 2016.

Buseck, P. R., Adachi, K., Gelencsér, A., Tompa, É., and Pósfai, M.: Ns-Soot: A Material-Based Term for Strongly Light-Absorbing Carbonaceous Particles, Aerosol Science and Technology, 48, 777-788, 10.1080/02786826.2014.919374, 2014.

Cappa, C. D., Onasch, T. B., Massoli, P., Worsnop, D. R., Bates, T. S., Cross, E. S., Davidovits, P., Hakala, J., Hayden, K. L., Jobson, B. T., Kolesar, K. R., Lack, D. A., Lerner, B. M., Li, S.-M., Mellon, D., Nuaaman, I., Olfert, J. S., Petäjä, T., Quinn, P. K., Song, C., Subramanian, R., Williams, E. J., and Zaveri, R. A.: Radiative Absorption Enhancements Due to the Mixing State of Atmospheric Black Carbon, Science, 337, 1078, 10.1126/science.1223447, 2012.

Carnerero, C., Pérez, N., Reche, C., Ealo, M., Titos, G., Lee, H.-K., Eun, H.-R., Park, Y.-H., Dada, L., Paasonen, P., Kerminen, V.-M., Mantilla, E., Escudero, M., Gómez-Moreno, F. J., Alonso-Blanco, E., Coz, E., Saiz-Lopez, A., Temime-Roussel, B., Marchand, N., Beddows, D. C. S., Harrison, R. M., Petäjä, T., Kulmala, M., Ahn, K.-H., Alastuey, A., and Querol, X.: Vertical and horizontal distribution of regional new particle formation events in Madrid, Atmospheric Chemistry and Physics, 18, 16601-16618, 10.5194/acp-18-

374   16601-2018, 2018.

375   Chen, S., Xu, L., Zhang, Y., Chen, B., Wang, X., Zhang, X., Zheng, M., Chen, J., Wang, W., Sun, Y., Fu, P.,
376   Wang, Z., and Li, W.: Direct observations of organic aerosols in common wintertime hazes in North China:
377   insights into direct emissions from Chinese residential stoves, Atmospheric Chemistry and Physics, 17,
378   1259-1270, 10.5194/acp-17-1259-2017, 2017.

379   Chen, Y., Ebenstein, A., Greenstone, M., and Li, H.: Evidence on the impact of sustained exposure to air
380   pollution on life expectancy from China's Huai River policy, Proc Natl Acad Sci U S A, 110, 12936-12941,
381   10.1073/pnas.1300018110, 2013.

382   China, S., Mazzoleni, C., Gorkowski, K., Aiken, A. C., and Dubey, M. K.: Morphology and mixing state of
383   individual freshly emitted wildfire carbonaceous particles, Nat Commun, 4, 2122,
384   10.1038/ncomms3122, 2013.

385   China, S., Mazzoleni, C., Gorkowski, K., Aiken, A.C. and Dubey, M.K., 2013. Morphology and mixing state
386   of individual freshly emitted wildfire carbonaceous particles. Nat Commun, 4: 2122.

387   China, S., Scarnato, B., Owen, R. C., Zhang, B., Ampadu, M. T., Kumar, S., Dzepina, K., Dziobak, M. P.,
388   Fialho, P., Perlinger, J. A., Hueber, J., Helmig, D., Mazzoleni, L. R., and Mazzoleni, C.: Morphology and
389   mixing state of aged soot particles at a remote marine free troposphere site: Implications for optical
390   properties, Geophysical Research Letters, 42, 1243-1250, 10.1002/2014gl062404, 2015.

391   De Marco, A., Proietti, C., Anav, A., Ciancarella, L., D'Elia, I., Fares, S., Fornasier, M. F., Fusaro, L., Gualtieri,
392   M., Manes, F., Marchetto, A., Mircea, M., Paoletti, E., Piersanti, A., Rogora, M., Salvati, L., Salvatori, E.,
393   Screpanti, A., Vialetto, G., Vitale, M., and Leonardi, C.: Impacts of air pollution on human and ecosystem
394   health, and implications for the National Emission Ceilings Directive: Insights from Italy, Environ Int, 125,
395   320-333, 10.1016/j.envint.2019.01.064, 2019.

396   Ebert, M., Weigel, R., Kandler, K., Günther, G., Molleker, S., Grooß, J. U., Vogel, B., Weinbruch, S., and
397   Borrmann, S.: Chemical analysis of refractory stratospheric aerosol particles collected within the arctic
398   vortex and inside polar stratospheric clouds, Atmos. Chem. Phys., 16, 8405-8421,502 10.5194/acp-16-
399   8405-2016, 2016.

400   Gao, J., Peng, X., Chen, G., Xu, J., Shi, G. L., Zhang, Y. C., and Feng, Y. C.: Insights into the chemical
401   characterization and sources of PM(2.5) in Beijing at a 1-h time resolution, Sci Total Environ, 542, 162-
402   171, 10.1016/j.scitotenv.2015.10.082, 2016.

403   Guo, S., Hu, M., Zamora, M. L., Peng, J., Shang, D., Zheng, J., Du, Z., Wu, Z., Shao, M., Zeng, L., Molina,
404   M. J., and Zhang, R.: Elucidating severe urban haze formation in China, Proc Natl Acad Sci U S A, 111,
405   17373-17378, 10.1073/pnas.1419604111, 2014.

406   Heald, C. L., Jacob, D. J., Park, R. J., Alexander, B., Fairlie, T. D., Yantosca, R. M., and Chu, D. A.: Transpacific
407   transport of Asian anthropogenic aerosols and its impact on surface air quality in the United States,
408   Journal of Geophysical Research, 111, 10.1029/2005jd006847, 2006.

409   Hoffer, A., Toth, A., Nyiro-Kosa, I., Posfai, M., and Gelencser, A.: Light absorption properties of
410   laboratory-generated tar ball particles, Atmospheric Chemistry and Physics, 16, 239-246, 10.5194/acp-
411   16-239-2016, 2016.

Hou, C., Shao, L., Hu, W., Zhang, D., Zhao, C., Xing, J., Huang, X., and Hu, M.: Characteristics and aging of traffic-derived particles in a highway tunnel at a coastal city in southern China, Sci Total Environ, 619-620, 1385-1393, 10.1016/j.scitotenv.2017.11.165, 2018.

Huang, R. J., Zhang, Y., Bozzetti, C., Ho, K. F., Cao, J. J., Han, Y., Daellenbach, K. R., Slowik, J. G., Platt, S. M., Canonaco, F., Zotter, P., Wolf, R., Pieber, S. M., Bruns, E. A., Crippa, M., Ciarelli, G., Piazzalunga, A., Schwikowski, M., Abbaszade, G., Schnelle-Kreis, J., Zimmermann, R., An, Z., Szidat, S., Baltensperger, U., El Haddad, I., and Prevot, A. S.: High secondary aerosol contribution to particulate pollution during haze events in China, Nature, 514, 218-222, 10.1038/nature13774, 2014.

Jacobson, M. Z.: Strong radiative heating due to the mixing state of black carbon in atmospheric aerosols, Nature, 409, 695-697, 10.1038/35055518, 2001.

Kahnert, M.: Modelling radiometric properties of inhomogeneous mineral dust particles: Applicability and limitations of effective medium theories, Journal of Quantitative Spectroscopy and Radiative Transfer, 152, 16-27, 10.1016/j.jqsrt.2014.10.025, 2015.

Kerminen, V. M., Paramonov, M., Anttila, T., Riipinen, I., Fountoukis, C., Korhonen, H., Asmi, E., Laakso, L., Lihavainen, H., Swietlicki, E., Svenningsson, B., Asmi, A., Pandis, S. N., Kulmala, M., and Petäjä, T.: Cloud condensation nuclei production associated with atmospheric nucleation: a synthesis based on existing literature and new results, Atmospheric Chemistry and Physics, 12, 12037-12059, 10.5194/acp-12-12037-2012, 2012.

Khalizov, A. F., Xue, H., Wang, L., Zheng, J., and Zhang, R.: Enhanced Light Absorption and Scattering by Carbon Soot Aerosol Internally Mixed with Sulfuric Acid, The Journal of Physical Chemistry A, 113, 1066-1074, 10.1021/jp807531n, 2009.

Kotthaus, S., O'Connor, E., Münkel, C., Charlton-Perez, C., Haeffelin, M., Gabey, A. M., and Grimmond, C. S. B.: Recommendations for processing atmospheric attenuated backscatter profiles from Vaisala CL31 ceilometers, Atmos. Meas. Tech., 9, 3769-3791, 10.5194/amt-9-3769-2016, 2016.

Kotthaus, S., and Grimmond, C. S. B.: Atmospheric boundary-layer characteristics from ceilometer measurements. Part 1: A new method to track mixed layer height and classify clouds, Quarterly Journal of the Royal Meteorological Society, 144, 1525-1538, 10.1002/qj.3299, 2018.

Laskin, A., Gilles, M. K., Knopf, D. A., Wang, B., and China, S.: Progress in the Analysis of Complex Atmospheric Particles, Annu Rev Anal Chem (Palo Alto Calif), 9, 117-143, 10.1146/annurev-anchem-071015-041521, 2016.

Lelieveld, J., Evans, J. S., Fnais, M., Giannadaki, D., and Pozzer, A.: The contribution of outdoor air pollution sources to premature mortality on a global scale, Nature, 525, 367-371, 10.1038/nature15371, 2015.

Li, J., Du, H., Wang, Z., Sun, Y., Yang, W., Li, J., Tang, X., and Fu, P.: Rapid formation of a severe regional winter haze episode over a mega-city cluster on the North China Plain, Environ Pollut, 223, 605-615, 10.1016/j.envpol.2017.01.063, 2017a.

Li, W., and Shao, L.: Transmission electron microscopy study of aerosol particles from the brown hazes in northern China, Journal of Geophysical Research, 114, 10.1029/2008jd011285, 2009.

Li, W., Shi, Z., Zhang, D., Zhang, X., Li, P., Feng, Q., Yuan, Q., and Wang, W.: Haze particles over a coal-burning region in the China Loess Plateau in winter: Three flight missions in December 2010, Journal of Geophysical Research: Atmospheres, 117, n/a-n/a, 10.1029/2012jd017720, 2012.

Li, W., Shao, L., Zhang, D., Ro, C.-U., Hu, M., Bi, X., Geng, H., Matsuki, A., Niu, H., and Chen, J.: A review of single aerosol particle studies in the atmosphere of East Asia: morphology, mixing state, source, and heterogeneous reactions, Journal of Cleaner Production, 112, 1330-1349, 10.1016/j.jclepro.2015.04.050, 2016a.

Li, W., Sun, J., Xu, L., Shi, Z., Riemer, N., Sun, Y., Fu, P., Zhang, J., Lin, Y., Wang, X., Shao, L., Chen, J., Zhang, X., Wang, Z., and Wang, W.: A conceptual framework for mixing structures in individual aerosol particles, Journal of Geophysical Research: Atmospheres, 121, 13,784-713,798, 10.1002/2016jd025252, 2016b.

Li, Z., Lee, K.-H., Wang, Y., Xin, J., and Hao, W.-M.: First observation-based estimates of cloud-free aerosol radiative forcing across China, 115, 10.1029/2009jd013306, 2010.

Li, Z., Guo, J., Ding, A., Liao, H., Liu, J., Sun, Y., Wang, T., Xue, H., Zhang, H., and Zhu, B.: Aerosol and boundary-layer interactions and impact on air quality, National Science Review, 4, 810-833, 10.1093/nsr/nwx117, 2017b.

Liu, L., Zhang, J., Zhang, Y.X., Wang, Y.Y., Xu, L., Yuan, Q., Liu, D.T., Sun, Y.L., Fu, P.Q., Shi, Z.B., and Li, W.J.: Persistent residential burning-related primary organic particles during wintertime hazes in North China: insights into their aging and optical changes, Atmospheric chemistry and physics, 21, 2251-2265, 10.5194/acp-21-2251-2021, 2021.

Liu, S., Aiken, A. C., Gorkowski, K., Dubey, M. K., Cappa, C. D., Williams, L. R., Herndon, S. C., Massoli, P., Fortner, E. C., Chhabra, P. S., Brooks, W. A., Onasch, T. B., Jayne, J. T., Worsnop, D. R., China, S., Sharma, N., Mazzoleni, C., Xu, L., Ng, N. L., Liu, D., Allan, J. D., Lee, J. D., Fleming, Z. L., Mohr, C., Zotter, P., Szidat, S., and Prévôt, A. S. H.: Enhanced light absorption by mixed source black and brown carbon particles in UK winter, Nature Communications, 6, 8435, 10.1038/ncomms9435. https://www.nature.com/articles/ncomms9435#supplementary-information, 2015.

Liu, Z., Hu, B., Zhang, J., Yu, Y., and Wang, Y.: Characteristics of aerosol size distributions and chemical compositions during wintertime pollution episodes in Beijing, Atmospheric Research, 168, 1-12, 10.1016/j.atmosres.2015.08.013, 2016.

Meng, Z. Y., Ding, G. A., Xu, X. B., Xu, X. D., Yu, H. Q., and Wang, S. F.: Vertical distributions of SO(2) and NO(2) in the lower atmosphere in Beijing urban areas, China, Sci Total Environ, 390, 456-465, 10.1016/j.scitotenv.2007.10.012, 2008.

Merikallio, S., Lindqvist, H., Nousiainen, T., and Kahnert, M.: Modelling light scattering by mineral dust using spheroids: assessment of applicability, Atmospheric Chemistry and Physics, 11, 5347-5363, 10.5194/acp-11-5347-2011, 2011.

Müller, A., Miyazaki, Y., Aggarwal, S. G., Kitamori, Y., Boreddy, S. K. R., and Kawamura, K.: Effects of chemical composition and mixing state on size‑resolved hygroscopicity and cloud condensation nuclei activity of submicron aerosols at a suburban site in northern Japan in summer, Journal of Geophysical Research: Atmospheres, 122, 9301-9318, 10.1002/2017jd027286, 2017.

Niu, H., Shao, L., and Zhang, D.: Soot particles at an elevated site in eastern China during the passage of

489 a strong cyclone, Sci Total Environ, 430, 217-222, 10.1016/j.scitotenv.2012.04.050, 2012.

490 Niu, H., Hu, W., Zhang, D., Wu, Z., Guo, S., Pian, W., Cheng, W., and Hu, M.: Variations of fine particle
491 physiochemical properties during a heavy haze episode in the winter of Beijing, Sci Total Environ, 571,
492 103-109, 10.1016/j.scitotenv.2016.07.147, 2016.

493 Peng, J., Hu, M., Guo, S., Du, Z., Zheng, J., Shang, D., Levy Zamora, M., Zeng, L., Shao, M., Wu, Y. S., Zheng,
494 J., Wang, Y., Glen, C. R., Collins, D. R., Molina, M. J., and Zhang, R.: Markedly enhanced absorption and
495 direct radiative forcing of black carbon under polluted urban environments, Proc Natl Acad Sci U S A,
496 113, 4266-4271, 10.1073/pnas.1602310113, 2016.

497 Petaja, T., Jarvi, L., Kerminen, V. M., Ding, A. J., Sun, J. N., Nie, W., Kujansuu, J., Virkkula, A., Yang, X. Q.,
498 Fu, C. B., Zilitinkevich, S., and Kulmala, M.: Enhanced air pollution via aerosol-boundary layer feedback
499 in China, Sci Rep, 6, 18998, 10.1038/srep18998, 2016.

500 Platis, A., Altstädter, B., Wehner, B., Wildmann, N., Lampert, A., Hermann, M., Birmili, W., and Bange, J.:
501 An Observational Case Study on the Influence of Atmospheric Boundary-Layer Dynamics on New
502 Particle Formation, Boundary-Layer Meteorology, 158, 67-92, 10.1007/s10546-015-0084-y, 2015.

503 Qi, X., Ding, A., Nie, W., Chi, X., Huang, X., Xu, Z., Wang, T., Wang, Z., Wang, J., Sun, P., Zhang, Q., Huo, J.,
504 Wang, D., Bian, Q., Zhou, L., Zhang, Q., Ning, Z., Fei, D., Xiu, G., and Fu, Q.: Direct measurement of new
505 particle formation based on tethered airship around the top of the planetary boundary layer in eastern
506 China, Atmospheric Environment, 209, 92-101, 10.1016/j.atmosenv.2019.04.024, 2019.

507 Ramanathan, V., Crutzen, P. J., Mitra, A. P., and Sikka, D.: The Indian Ocean Experiment and the Asian
508 Brown Cloud, Curr. Sci., 83, 947-955, 2002.

509 Rodriguez-Navarro, C., di Lorenzo, F., and Elert, K.: Mineralogy and physicochemical features of Saharan
510 dust wet deposited in the Iberian Peninsula during an extreme red rain event, Atmospheric Chemistry
511 and Physics, 18, 10089-10122, 10.5194/acp-18-10089-2018, 2018.

512 Saliba, G., Subramanian, R., Saleh, R., Ahern, A. T., Lipsky, E. M., Tasoglou, A., Sullivan, R. C., Bhandari,
513 J., Mazzoleni, C., and Robinson, A. L.: Optical properties of black carbon in cookstove emissions coated
514 with secondary organic aerosols: Measurements and modeling, Aerosol Science and Technology, 50,
515 1264-1276, 10.1080/02786826.2016.1225947, 2016.

516 Scarnato, B. V., Vahidinia, S., Richard, D. T., and Kirchstetter, T. W.: Effects of internal mixing and
517 aggregate morphology on optical properties of black carbon using a discrete dipole approximation
518 model, Atmospheric Chemistry and Physics, 13, 5089-5101, 10.5194/acp-13-5089-2013, 2013.

519 Schneider, C. A., Rasband, W. S., and Eliceiri, K. W.: NIH Image to ImageJ: 25 years of image analysis,
520 Nature Methods, 9, 671-675, 10.1038/nmeth.2089, 2012.

521 Shao, L., Hou, C., Geng, C., Liu, J., Hu, Y., Wang, J., Jones, T., Zhao, C., and BéruBé, K.: The oxidative
522 potential of PM 10 from coal, briquettes and wood charcoal burnt in an experimental domestic stove,
523 Atmospheric Environment, 127, 372-381, 10.1016/j.atmosenv.2015.12.007, 2016.

524 Shao, L., Hu, Y., Shen, R., Schafer, K., Wang, J., Wang, J., Schnelle-Kreis, J., Zimmermann, R., BeruBe, K.,
525 and Suppan, P.: Seasonal variation of particle-induced oxidative potential of airborne particulate matter
526 in Beijing, Sci Total Environ, 579, 1152-1160, 10.1016/j.scitotenv.2016.11.094, 2017.

Sharma, N., China, S., Bhandari, J., Gorkowski, K., Dubey, M., Zaveri, R. A., and Mazzoleni, C.: Physical Properties of Aerosol Internally Mixed With Soot Particles in a Biogenically Dominated Environment in California, Geophysical Research Letters, 45, 11,473-411,482, 10.1029/2018gl079404, 2018.

Shi, Z., Vu, T., Kotthaus, S., Harrison, R. M., Grimmond, S., Yue, S., Zhu, T., Lee, J., Han, Y., Demuzere, M., Dunmore, R. E., Ren, L., Liu, D., Wang, Y., Wild, O., Allan, J., Acton, W. J., Barlow, J., Barratt, B., Beddows, D., Bloss, W. J., Calzolai, G., Carruthers, D., Carslaw, D. C., Chan, Q., Chatzidiakou, L., Chen, Y., Crilley, L., Coe, H., Dai, T., Doherty, R., Duan, F., Fu, P., Ge, B., Ge, M., Guan, D., Hamilton, J. F., He, K., Heal, M., Heard, D., Hewitt, C. N., Hollaway, M., Hu, M., Ji, D., Jiang, X., Jones, R., Kalberer, M., Kelly, F. J., Kramer, L., Langford, B., Lin, C., Lewis, A. C., Li, J., Li, W., Liu, H., Liu, J., Loh, M., Lu, K., Lucarelli, F., Mann, G., McFiggans, G., Miller, M. R., Mills, G., Monk, P., Nemitz, E., amp, apos, Connor, F., Ouyang, B., Palmer, P. I., Percival, C., Popoola, O., Reeves, C., Rickard, A. R., Shao, L., Shi, G., Spracklen, D., Stevenson, D., Sun, Y., Sun, Z., Tao, S., Tong, S., Wang, Q., Wang, W., Wang, X., Wang, X., Wang, Z., Wei, L., Whalley, L., Wu, X., Wu, Z., Xie, P., Yang, F., Zhang, Q., Zhang, Y., Zhang, Y., and Zheng, M.: Introduction to the special issue "In-depth study of air pollution sources and processes within Beijing and its surrounding region (APHH-Beijing)", Atmospheric Chemistry and Physics, 19, 7519-7546, 10.5194/acp-19-7519-2019, 2019.

Shou, Y., Huang, Y., Zhu, X., Liu, C., Hu, Y., and Wang, H.: A review of the possible associations between ambient PM2.5 exposures and the development of Alzheimer's disease, Ecotoxicol Environ Saf, 174, 344-352, 10.1016/j.ecoenv.2019.02.086, 2019.

Sorensen, C.M., 2001. Light Scattering by Fractal Aggregates: A Review. Aerosol Science and Technology, 35(2): 648-687.

Sun, Y., Zhuang, G., Tang, A., Wang, Y., and An, Z.: Chemical Characteristics of PM2.5 and PM10 in Haze−Fog Episodes in Beijing, Environmental Science & Technology, 40, 3148-3155, 10.1021/es051533g, 2006.

Sun, Y., Jiang, Q., Wang, Z., Fu, P., Li, J., Yang, T., and Yin, Y.: Investigation of the sources and evolution processes of severe haze pollution in Beijing in January 2013, Journal of Geophysical Research: Atmospheres, 119, 4380-4398, 10.1002/2014jd021641, 2014.

Sun, Y., Du, W., Wang, Q., Zhang, Q., Chen, C., Chen, Y., Chen, Z., Fu, P., Wang, Z., Gao, Z., and Worsnop, D. R.: Real-Time Characterization of Aerosol Particle Composition above the Urban Canopy in Beijing: Insights into the Interactions between the Atmospheric Boundary Layer and Aerosol Chemistry, Environ Sci Technol, 49, 11340-11347, 10.1021/acs.est.5b02373, 2015.

Sun, Y., Du, W., Fu, P., Wang, Q., Li, J., Ge, X., Zhang, Q., Zhu, C., Ren, L., Xu, W., Zhao, J., Han, T., Worsnop, D. R., and Wang, Z.: Primary and secondary aerosols in Beijing in winter: sources, variations and

processes, Atmospheric Chemistry and Physics, 16, 8309-8329, 10.5194/acp-16-8309-2016, 2016.

Sun, Y. L., Wang, Z. F., Fu, P. Q., Yang, T., Jiang, Q., Dong, H. B., Li, J., and Jia, J. J.: Aerosol composition, sources and processes during wintertime in Beijing, China, Atmospheric Chemistry and Physics, 13, 4577-4592, 10.5194/acp-13-4577-2013, 2013.

Tang, M., Cziczo, D. J., and Grassian, V. H.: Interactions of Water with Mineral Dust Aerosol: Water Adsorption, Hygroscopicity, Cloud Condensation, and Ice Nucleation, Chem Rev, 116, 4205-4259, 10.1021/acs.chemrev.5b00529, 2016.

Tao, J., Zhang, L., Cao, J., and Zhang, R.: A review of current knowledge concerning PM$_{2.5}$ chemical composition, aerosol optical properties and their relationships across China, Atmospheric Chemistry and Physics, 17, 9485-9518, 10.5194/acp-17-9485-2017, 2017.

Unga, F., Choël, M., Derimian, Y., Deboudt, K., Dubovik, O., and Goloub, P.: Microscopic Observations of Core‑Shell Particle Structure and Implications for Atmospheric Aerosol Remote Sensing, Journal of Geophysical Research: Atmospheres, 123, 13,944-913,962, 10.1029/2018jd028602, 2018.

Wang, G., Zhang, R., Gomez, M. E., Yang, L., Levy Zamora, M., Hu, M., Lin, Y., Peng, J., Guo, S., Meng, J., Li, J., Cheng, C., Hu, T., Ren, Y., Wang, Y., Gao, J., Cao, J., An, Z., Zhou, W., Li, G., Wang, J., Tian, P., Marrero-Ortiz, W., Secrest, J., Du, Z., Zheng, J., Shang, D., Zeng, L., Shao, M., Wang, W., Huang, Y., Wang, Y., Zhu, Y., Li, Y., Hu, J., Pan, B., Cai, L., Cheng, Y., Ji, Y., Zhang, F., Rosenfeld, D., Liss, P. S., Duce, R. A., Kolb, C. E., and Molina, M. J.: Persistent sulfate formation from London Fog to Chinese haze, Proc Natl Acad Sci U S A, 113, 13630-13635, 10.1073/pnas.1616540113, 2016.

Wang, Q., Sun, Y., Xu, W., Du, W., Zhou, L., Tang, G., Chen, C., Cheng, X., Zhao, X., Ji, D., Han, T., Wang, Z., Li, J., and Wang, Z.: Vertically resolved characteristics of air pollution during two severe winter haze episodes in urban Beijing, China, Atmospheric Chemistry and Physics, 18, 2495-2509, 10.5194/acp-18-2495-2018, 2018.

Wang, W., Shao, L., Guo, M., Hou, C., Xing, J., and Wu, F.: Physicochemical Properties of Individual Airborne Particles in Beijing during Pollution Periods, Aerosol and Air Quality Research, 17, 3209-3219, 10.4209/aaqr.2017.03.0116, 2017.

Wang, X., Cotter, E., Iyer, K. N., Fang, J., Williams, B. J., and Biswas, P.: Relationship between pyrolysis products and organic aerosols formed during coal combustion, Proceedings of the Combustion Institute, 35, 2347-2354, 10.1016/j.proci.2014.07.073, 2015.

Wang, Y., Yao, L., Wang, L., Liu, Z., Ji, D., Tang, G., Zhang, J., Sun, Y., Hu, B., and Xin, J.: Mechanism for the formation of the January 2013 heavy haze pollution episode over central and eastern China, Science China Earth Sciences, 57, 14-25, 10.1007/s11430-013-4773-4, 2013.

Wehner, B., Siebert, H., Ansmann, A., Ditas, F., Seifert, P., Stratmann, F., Wiedensohler, A., Apituley, A., Shaw, R. A., Manninen, H. E., and Kulmala, M.: Observations of turbulence-induced new particle formation in the residual layer, Atmospheric Chemistry and Physics, 10, 4319-4330, 10.5194/acp-10-4319-2010, 2010.

Li, W., Xu, L., Liu, X., Zhang, J., Lin, Y., Yao, X., Gao, H., Zhang, D., Chen, J., Wang, W., Harrison, R. M., Zhang, X., Shao, L., Fu, P.: Athanasios Nenes, and Zongbo Shi: Air pollution—aerosol interactions produce more bioavailable iron for ocean ecosystems, Science Advance, 3, e1601749, 2017.

Xia, Y., Guan, D., Meng, J., Li, Y., and Shan, Y.: Assessment of the pollution—health—economics nexus in China, Atmospheric Chemistry and Physics, 18, 14433-14443, 10.5194/acp-18-14433-2018, 2018.

Xu, L., Liu, L., Zhang, J., Zhang, Y., Ren, Y., Wang, X., and Li, W.: Morphology, Composition, and Mixing State of Individual Aerosol Particles in Northeast China during Wintertime, Atmosphere, 8, 10.3390/atmos8030047, 2017.

Xu, L., Zhang, D., and Li, W.: Microscopic comparison of aerosol particles collected at an urban site in North China and a coastal site in Japan, Sci Total Environ, 669, 948-954, 10.1016/j.scitotenv.2019.03.163,

2019.

Yuan, Q., Li, W., Zhou, S., Yang, L., Chi, J., Sui, X., and Wang, W.: Integrated evaluation of aerosols during haze-fog episodes at one regional background site in North China Plain, Atmospheric Research, 156, 102-110, 10.1016/j.atmosres.2015.01.002, 2015.

Zhang, D., Chen, B., Yamada, M., Niu, H., Wang, B., Iwasaka, Y., and Shi, G.: Elevated soot layer in polluted atmosphere: A case study in Beijing, Journal of the Meteorological Society of Japan., 90, 361-375, 10.2151/jmsj.2012-302, 2012.

Zhang, J., Liu, L., Wang, Y., Ren, Y., Wang, X., Shi, Z., Zhang, D., Che, H., Zhao, H., Liu, Y., Niu, H., Chen, J., Zhang, X., Lingaswamy, A. P., Wang, Z., and Li, W.: Chemical composition, source, and process of urban aerosols during winter haze formation in Northeast China, Environ Pollut, 231, 357-366, 10.1016/j.envpol.2017.07.102, 2017.

Zhang, J., Liu, L., Xu, L., Lin, Q., Zhao, H., Wang, Z., Guo, S., Hu, M., Liu, D., Shi, Z., Huang, D., and Li, W.: Exploring wintertime regional haze in northeast China: role of coal and biomass burning, Atmos. Chem. Phys., 20, 5355-5372, 10.5194/acp-20-5355-2020, 2020.

Zhang, Q., Ma, X., Tie, X., Huang, M., and Zhao, C.: Vertical distributions of aerosols under different weather conditions: Analysis of in-situ aircraft measurements in Beijing, China, Atmospheric Environment, 43, 5526-5535, https://doi.org/10.1016/j.atmosenv.2009.05.037, 2009.

Zhou, W., Sun, Y., Xu, W., Zhao, X., Wang, Q., Tang, G., Zhou, L., Chen, C., Du, W., Zhao, J., Xie, C., Fu, P., and Wang, Z.: Vertical Characterization of Aerosol Particle Composition in Beijing, China: Insights From 3-Month Measurements With Two Aerosol Mass Spectrometers, Journal of Geophysical Research: Atmospheres, 123, 13,016-013,029, 10.1029/2018jd029337, 2018a.

Zhou, W., Wang, Q., Zhao, X., Xu, W., Chen, C., Du, W., Zhao, J., Canonaco, F., Prévôt, A. S. H., Fu, P., Wang, Z., Worsnop, D. R., and Sun, Y.: Characterization and source apportionment of organic aerosol at 260 m on a meteorological tower in Beijing, China, Atmospheric Chemistry and Physics, 18, 3951-3968, 10.5194/acp-18-3951-2018, 2018b.

Zhu, J., Crozier, P. A., and Anderson, J. R.: Characterization of light-absorbing carbon particles at three altitudes in East Asian outflow by transmission electron microscopy, Atmospheric Chemistry and Physics, 13, 6359-6371, 10.5194/acp-13-6359-2013, 2013.

633   Table 1 Sample information and meteorological conditions

Sample ID①	Date (2016)	Time ②	$PM_{2.5}$ ($\mu g\ m^{-3}$)	SO_2 ($\mu g\ m^{-3}$)	NO_2 ($\mu g\ m^{-3}$)	O_3 ($\mu g\ m^{-3}$)	RH (%)	T (℃)	MLH (m)③
Z1-1	12/1	9:10	12④	2	48	37	24	6	--
Z2-1	12/1	8:40	--	--	--	--	--	--	194
Z1-2	12/2	1:00	110	25	109	3	55	2	--
Z2-2	12/2	1:00	--	--	--	--	--	--	141
Z1-3	12/2	9:10	24	20	134	2	50	3	--
Z2-3	12/2	8:40	--	--	--	--	--	--	134
Z1-4	12/3	1:53	142	36	102	6	79	-1	--
Z2-4	12/3	3:00	--	--	--	--	--	--	232
Z1-5	12/4	1:04	530	14	180	4	93	1	--
Z2-5	12/4	3:00	--	--	--	--	--	--	136
Z1-6	12/5	2:00	86	8	21	53	75	2	--
Z2-6	12/5	2:00	--	--	--	--	--	--	114
Z1-7	12/8	9:10	187	2	16	72	86	2	--
Z2-7	12/8	8:40	--	--	--	--	--	--	191
Z1-8	12/9	9:20	12	8	67	12	33	2	--
Z2-8	12/9	8:30	--	--	--	--	--	--	250

634   ①Samples are collected at two altitudes: Z1 is 2 m above ground and Z2 is 280 m above ground.

635   ② Sampling duration ranges from 30 seconds to less than 5 minutes depending on the PM pollution.

636   ③ MLH represents the mixed layer height and the data are 15minutes average; MLH is less than

637   280 m and the samples collected at Z2 represent samples above the mixed layer. ④ If $PM_{2.5}$ mass

638   concentration is less than 75 $\mu g\ m^{-3}$, samples are classified as non-haze samples and if $PM_{2.5}$ mass

639   concentration is more than 75 $\mu g\ m^{-3}$, samples are classified as haze samples.

640 Table 2 Classification and characteristics of individual particle types.

Particle type	Elemental composition	Morphology	Possible sources
Soot particles	C and minor amounts of O, Si.	Chain-like or compact C-dominated aggregates.	Incomplete combustion of biomass and fossil fuel.
Primary organic particles	C and O with minor amounts of Si, K, S, Cl.	Spherical, near spherical or irregular shapes.	Mainly from Combustion process of biomass and fossil fuels.
Mineral particles	O, Si, Al, Ca, Fe, Na, K, Mg, Ti, and S.	Irregular shapes.	Re-suspended from soil dust, road dust, and construction dust.
Metal particles	Fe, Zn, Mn, Ti, and Pb.	Spherical or irregular shapes.	Industries, coal-fired power plants and oil refineries.
S-rich particles	S and O with minor amounts of N, K.	Spherical, near spherical or irregular shapes.	Secondary aerosol formation.
Organic mixed with Sulfur-rich particles	C, O, and S with minor amounts of N, K or Cl.	Irregular shapes.	Secondary aerosol reaction.
Other mixed particles	Complex elemental composition.	Irregular shapes with different particle types.	Secondary aerosol reaction.

641

642 Table 3 Relative number percentage of individual particles.

Air qualities	Sample ID	Number	Metals	Minerals	POA	S-rich	Soot	OP-S	Other
Non-haze periods	Z1-1	114	2.6	30.7	19.3	36.0	5.3	1.8	4.4
	Z2-1	113	1.8	12.4	16.8	56.6	10.6	0.9	0.9
	Z1-3	135	4.4	34.1	31.9	12.6	11.1	0.7	5.2
	Z2-3	118	2.5	23.7	45.8	17.0	4.2	2.5	4.2
	Z1-8	140	1.4	62.9	12.1	11.4	2.9	2.1	7.1
	Z2-8	119	3.4	33.6	19.3	18.5	17.7	0.0	7.6
	Ave (Z1)	389	2.8	42.5	21.1	20.0	6.4	1.6	5.6
	Ave (Z2)	350	2.6	23.2	27.3	30.7	10.8	1.1	4.2
Haze periods	Z1-2	123	2.4	21.1	42.3	17.1	7.3	2.4	7.3
	Z2-2	164	4.9	14.6	37.2	25.0	4.3	9.8	4.3
	Z1-4	160	0.6	28.8	30.6	8.8	13.8	9.4	8.1
	Z2-4	266	0.0	3.8	53.0	3.4	7.1	19.6	13.2
	Z1-5	461	0.9	6.5	18.9	22.1	7.6	31.5	12.6
	Z2-5	266	0.4	0.4	32.3	7.1	2.3	44.0	13.5
	Z1-6	237	2.5	11.0	21.5	48.5	2.1	6.8	7.6
	Z2-6	281	1.8	11.0	18.9	19.6	12.8	15.3	20.6
	Z1-7	168	1.8	23.2	28.0	20.8	2.4	15.5	8.3
	Z2-7	192	1.6	17.7	32.3	27.1	1.6	15.1	4.7
	Ave (Z1)	1149	1.7	18.1	28.3	23.5	6.6	13.1	8.8
	Ave (Z2)	1169	1.7	9.5	34.7	16.4	5.6	20.7	11.3

643
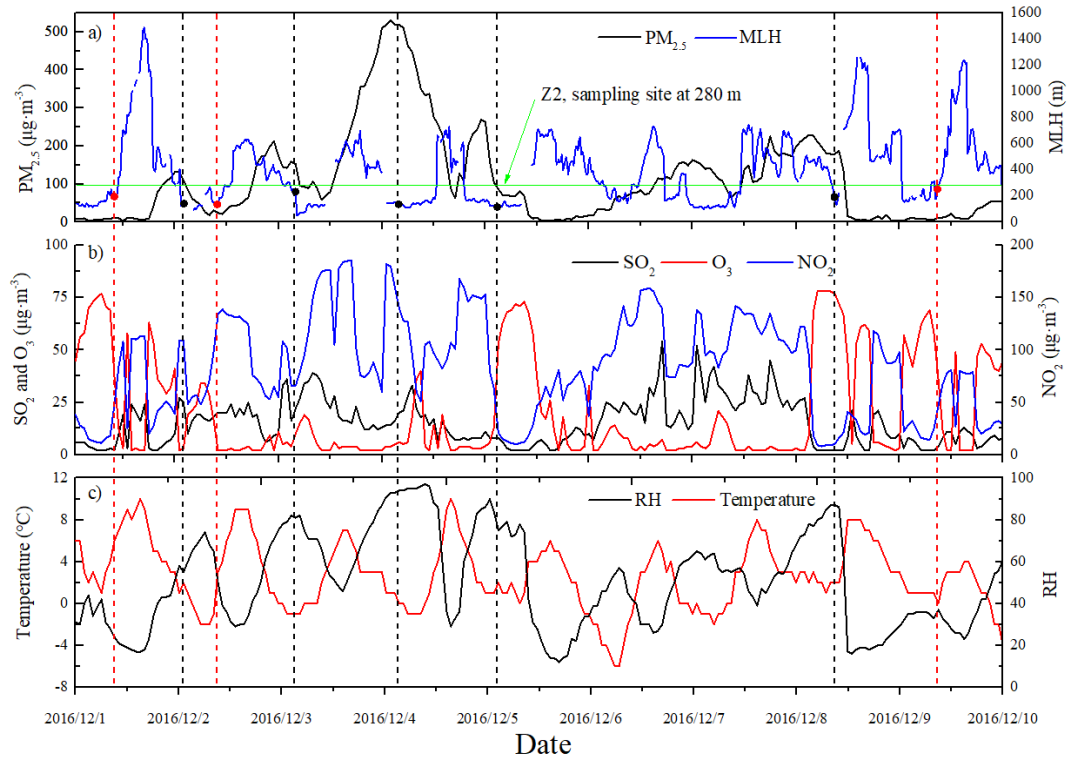
644

645 Fig. 1: The dashed lines represent the individual particle sampling times with red lines representing
646 non-haze samples and black lines haze samples. (a) Temporal variations of mixed layer height
647 (MLH) and $PM_{2.5}$ mass concentrations. The solid dots represent the MLH during the sampling times.
648 (b) Temporal variations of SO_2, NO_2, O_3 at ground level at the Olympic Park monitor site, which is
649 the closest national air quality monitor station to the sampling site (~1.5 km). (c) Temporal variations
650 of temperature (T) and relative humidity (RH) at ground level. Date was obtained from the Ministry
651 of Ecology and Environment of China (https://www.aqistudy.cn).

652
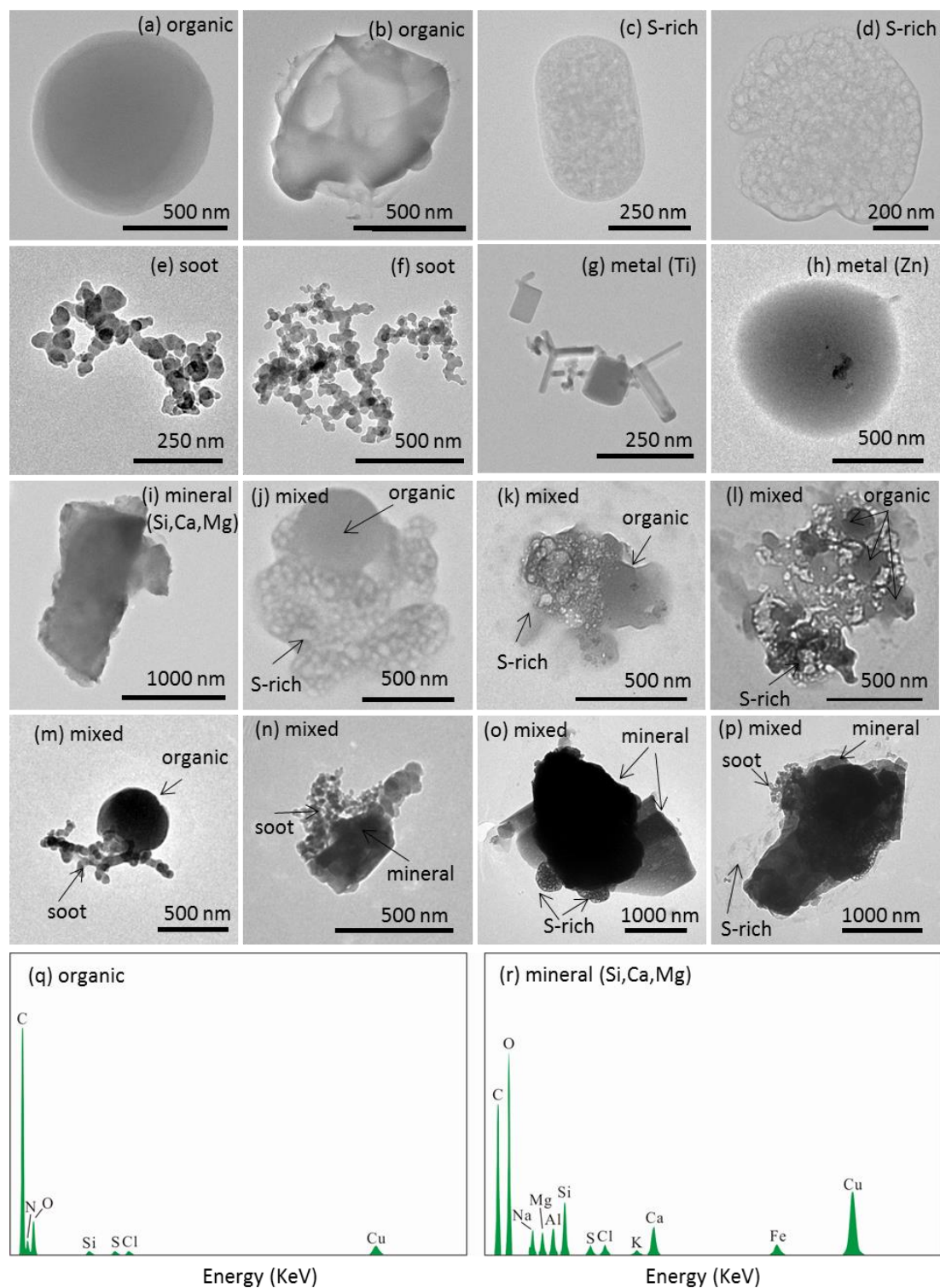
Fig. 2: Examples of morphologies and mixing characteristics of individual aerosol particles in winter in Beijing at ground level and above the mixed layer. (a) Spherical organic particle, (b) irregular shaped organic particle, (c-d) S-rich particles, (e-f) soot particles, (g-h) metal particles, (i) mineral particles, (j-l) OP-S mixed particles, and (m-p) other mixed particle types. (q) and (r) are EDS of (b) and (i). The difference between the particles in (b) and (i) is that organic particles (b) mainly composed C and O while minerals (i) mainly composed O, Si, Ca and Mg.

659
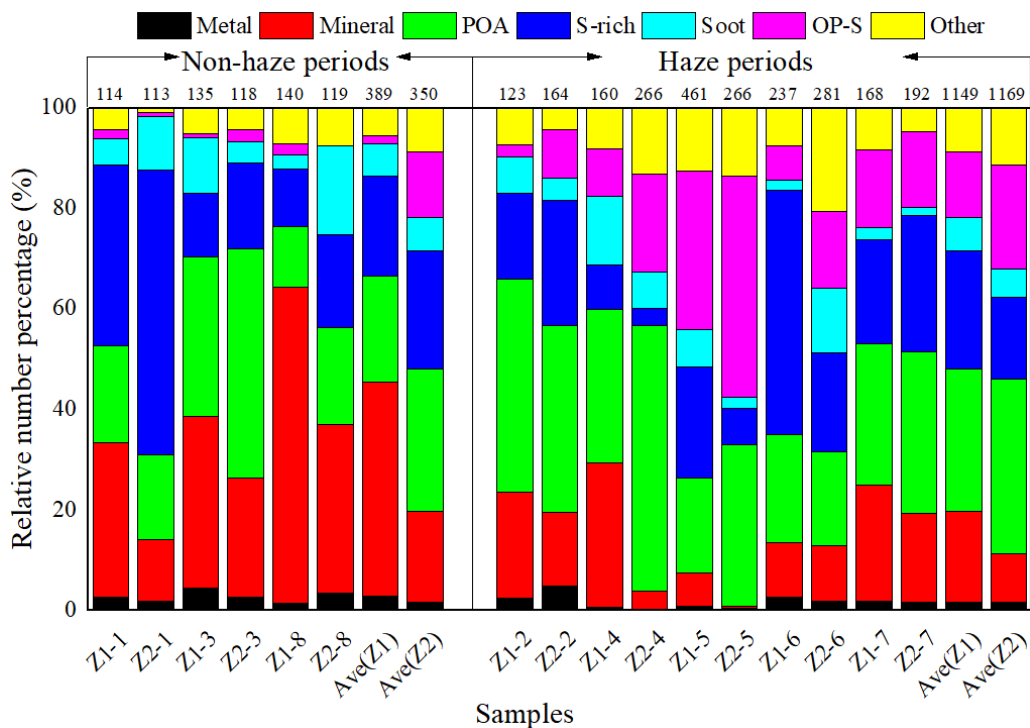
660
661   Fig. 3: Relative number percentage of different particle types at ground level (Z1) and above the
662   mixed layer height (Z2). The number above each bar represents the total particle number analyzed
663   in each sample.

664
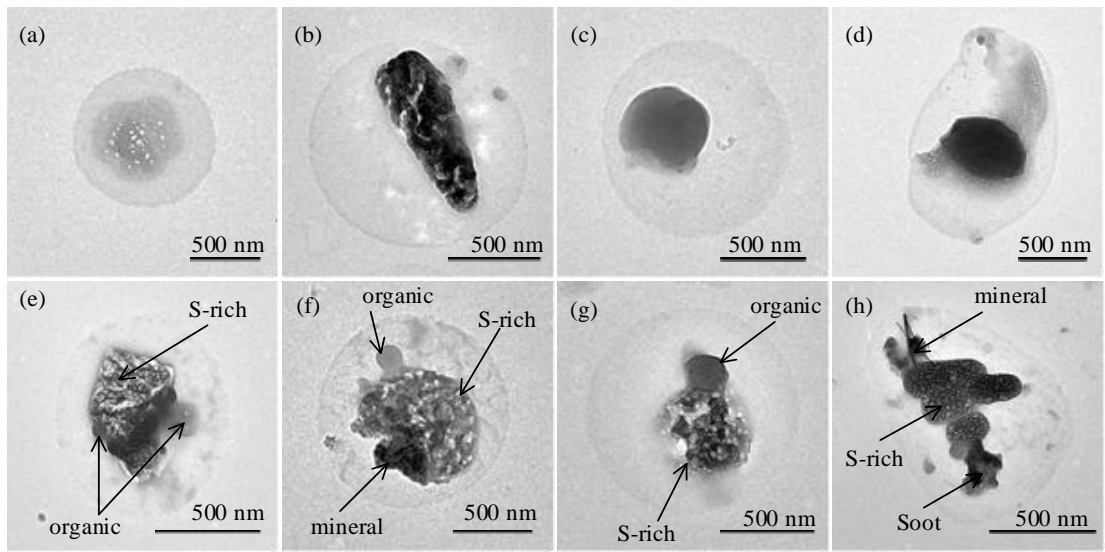
665 Fig. 4: Images of core-shell structured particles. (a-b) S-rich cores, (c-d) organic cores, and (e-h)

666 mixed cores.

667
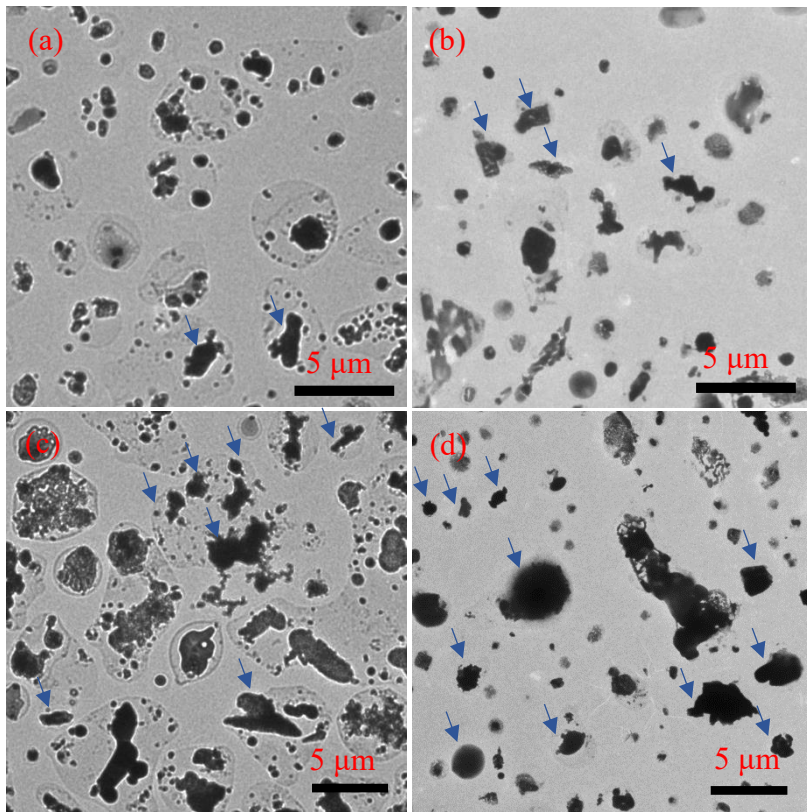
668 Fig. 5: Low magnification images of individual particles. (a) and (c) are particles above the mixed

669 layer (MLH) at different size ranges. (b) and (d) are particles at ground level at different size

670 ranges. More coated particles were found above the MLH. Arrows show part of the mineral

671 particles.

672
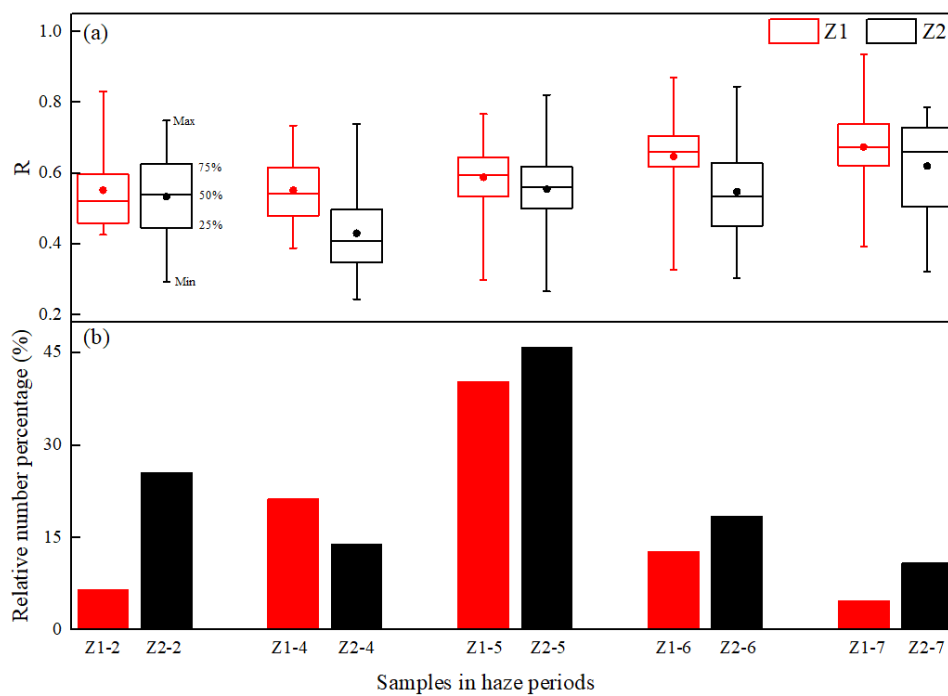
673

674 Fig. 6: (a) R is C/S ratio (D_{Aeq} ratio of the core to the whole particle including the shell) of particles

675 during haze periods at ground level (Z1) and above the mixed layer height (Z2); solid dots represent

676 the average value, and (b) the corresponding relative number percentage of core-shell structured

677 particles.

678
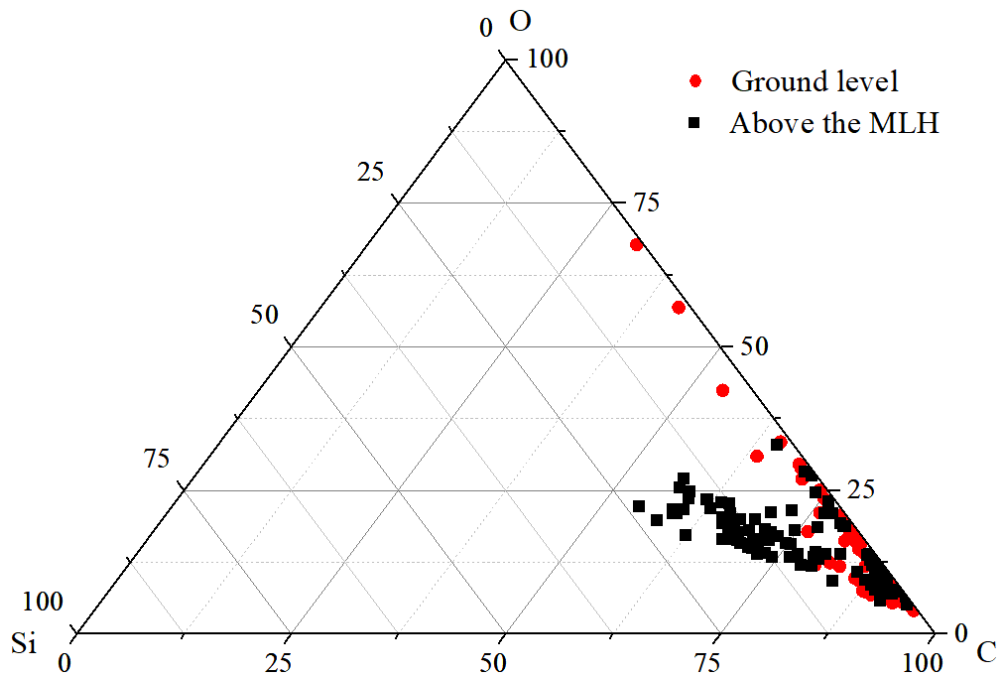
679   Fig. 7: Triangular diagram showing the weight ratio of C-O-Si of primary organic aerosols (POA)

680   at ground level and above the mixed layer height (MLH).